Multilayer film passivation for enhanced reliability of power semiconductor devices

Journal of Vacuum Science Technology B

Multi-layer film passivation for enhanced reliability of power semiconductor devices

Running title: Multi-layer film passivation for power semiconductor devices
Running Authors: Busca R. et al.

R. Busca[1,2,a)], D. Cimmino[1,2], S. Ferrero[1], L. Scaltrito[1], C. F. Pirri[1], G. Richieri[2], and R. Carta[2]

[1]DISAT, Polytechnic University of Turin, 10123 Turin, Italy
[2]Diodes Division, Vishay Intertechnology, Inc., 10071 Borgaro Torinese, Turin, Italy

[a)] Electronic mail: roberta.busca@vishay.com

Automotive requirements are becoming ever more severe in terms of device operation under high-stress and in harsh working conditions. In this context, passivation layers play a fundamental role in determining electrical performance and reliability. This study focuses on the primary and secondary passivation layers applied to state-of-the-art power devices and their influence on reliability. Power diodes assembled in standard module packages are used as test vehicles, and high-voltage temperature humidity bias tests are performed to stress the structures. A complete failure mode analysis highlights the phenomena behind the degradation of the passivation layers. Different passivation schemes are evaluated through the application of specific inorganic and organic combinations of layers. Finally, a summary of the typical degradation mechanisms and interactions is presented.

I. INTRODUCTION

Automotive customers are increasingly demanding diode and insulated-gate bipolar transistor robustness above the levels required by Automotive AEC Q101 standards. In parallel, higher device reliability is becoming a common requirement in industrial and commercial applications.[1] A number of studies have concentrated on device humidity robustness when assembled in the power modules commonly adopted in outdoor applications. Power modules have a relatively high moisture uptake because they are not hermetically sealed; the silicone gel widely used as an encapsulation material is not waterproof. For this reason, humidity can easily diffuse through the package and reach the semiconductor device, initiating a variety of deteriorating mechanisms. This eventually leads to progressive degradation of the electrical performance and, finally, failure. Hence, improved passivation that is able to protect the device termination from the external environment is an important objective.

A typical passivation scheme is composed of a combination of semi-resistive and dielectric layers made of inorganic and organic materials, each having particular chemical and physical characteristics. The way in which the whole passivation–termination structure reacts with external conditions and responds to thermal stress is therefore very complex. To understand the synergy between the various materials, a systematic study has been performed using a high-voltage temperature humidity bias (HV-THB) test. This test stresses the devices and stimulates particular failures. These failure modes are successively studied with various techniques in order to understand the different degradation mechanisms.

A. Passivation requirement and device-critical regions

Commonly, power semiconductor devices have two main structures: an active area and a termination. The active area is important for the current capability and dynamic behavior, whereas the termination plays an important role in sustaining breakdown, thus determining the rated blocking voltage value. A widely adopted concept for the termination region is the floating field limiting ring (FLR) structure. As an alternative, the junction termination extension represents an evolution towards a more efficient and smaller design.

In this field, multiple studies have attempted to improve device stability, especially for designs that are sensitive to process variations. Usually, novel designs are developed with the aid of 2D TCAD simulations. A more recent approach considers the design and passivation structure as an integrated ensemble that should be optimized simultaneously.

The passivation scheme needs to be able to sustain the maximum electric field to prevent the formation of any leakage path and improve the electric insulation under blocking conditions. The structure is composed of two main sections related to their functionality: primary and secondary passivation (see Fig. 1 for termination description). The primary passivation is in direct contact with the junction-diffused termination, and is typically composed of silicon oxide, resistive silicon, or semi-insulating polycrystalline silicon (SIPOS) and silicon nitride (Si_3N_4). Newer high-performance dielectric materials, such as diamond-like carbon, HfO_2, Al_2O_3, and Ta_2O_5, are becoming increasingly important in emerging SiC and GaN semiconductors.[2,3] The secondary passivation is

deposited on the first one to reinforce the die protection against mechanical damage and chemical contamination. Furthermore, it increases the surface electrical insulation and improves hermeticity. This film usually consists of multiple combinations of dielectric organic materials, among which polyimides (PIs), polybenzoxazines (PBOs), and benzocyclobutenes are the most popular.

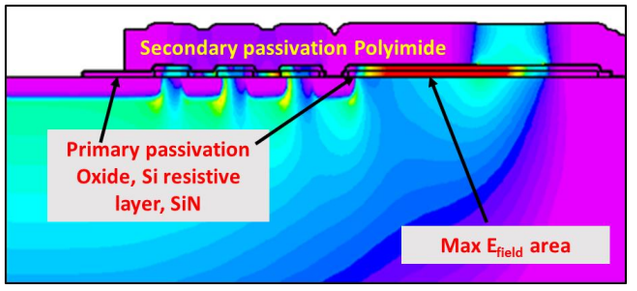

FIG. 1. Description of the HV planar termination, including primary and secondary passivation layers. Primary passivation is composed of oxide, silicon resistive layer, and silicon nitride. Secondary passivation is provided by a polyimide layer. The electric field distribution varies from a lower electric field (purple) to a higher electric field (red). The critical regions are located in the maximum electric field.

The advantage of organic films is that polymers have lower internal stress, less mechanical and thermal mismatch with respect to silicon, and more flexibility compared with inorganic passivation layers (e.g., thick silicon nitride). Thick silicon nitride layers, widely used in the past, suffer from crack formation, which causes premature device failures.

Several studies have reported HV-THB tests on high-power silicon devices.[1,2,4,5] These investigations highlight the connection between passivation layer degradation and the presence of high electric fields in specific regions of the devices. Moreover, the presence of humidity acts as an accelerant, allowing chemical–physical deterioration processes to occur more easily.[4]

II. EXPERIMENTAL SETUP AND METHODOLOGY

A. Test methodology validation

The current automotive THB standard test, also known as H3TRB in the AEC-Q101 semiconductor qualification framework, operates under fixed conditions of 85°C, 85% relative humidity (RH), and a maximum reverse bias (Vr) of 100 V, with a target requirement of no failures until 1000 h.[6]

For the purpose of this study, a further voltage stress is introduced with respect to the standard: the maximum reverse bias is increased to 80% of the nominal blocking voltage capability of the device, and the 100 V bias limitation is removed. A tool able to perform HV-THB testing has been developed with live leakage monitoring and a higher voltage bias of up to 600 V. With this setup, the testing conditions were set to 85°C, 85% RH, and Vr at 80%.[7]

Before the evaluation, a set of power diodes with a blocking voltage capability of 650 V and an FLR termination structure were used to validate the HV-THB capability to overstress the devices. This group of diodes presents a simple passivation structure composed of oxide, a silicon resistive layer as primary passivation, and an additional PI

layer as secondary passivation (Fig. 2). The devices were assembled in standard TO-247 plastic packages and in MTP power module packages. The latter were then subjected to HV-THB tests with 520 V reverse bias.

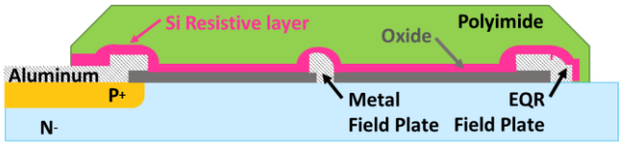

FIG. 2. Passivation structure of devices under test (typical HV planar termination). The structure is composed of oxide, silicon resistive layer, and PI. Aluminum metal field plate and equipotential ring (EQR) field plate are visible.

Two packages characterized by different water uptakes were used to understand the correlation between humidity and device degradation. Specifically, for the MTP power module, a weight difference of 1.9 g was measured after 24 h at 85% RH, evidencing a significant absorption. In contrast, no weight change was measured in the TO-247 package. Moreover, devices under test (DUTs) assembled in the plastic package showed slight signs of leakage shift after 500 h of testing, whereas the die assembled in power modules exhibited leakage degradation after only 168 h. It is important to underline that the same configuration of DUTs passed the standard AEC-Q101 H3TRB automotive test procedure.

After the tests, the diodes assembled in the TO-247 package were decapsulated using hot sulfuric acid at 150°C. This also dissolved the PI layer due to the lack of selectivity of the acid between the package and the organic film. The diodes assembled in the power modules were treated with DOWSIL 3522 at 40°C to remove the protective

silicone gel. In this case, the solvent did not affect the PI layer and it was still possible to analyze this secondary passivation coating.

A preliminary investigation of the samples was performed by optical microscopy using a Nikon Eclipse LV150. On the selected region, a multi-beam field-effect scanning electron microscope (FESEM) equipped with a focus ion beam (FIB) was used to prepare and analyze specific cross-sections (AURIGA, ZEISS, probe current range of 1 pA–29 nA and HV range of 2–30 kV).

The elemental composition was determined by energy dispersive X-ray (EDX) analysis carried out with a Supra 40 FESEM (ZEISS) with an Oxford INCA Energy 450 X-ray detector.

Optical microscope inspection indicated that the degradation looked different, but was located in the same position on both devices (Figs. 3a, 3b, 3c). Furthermore, the die from the power module exhibited bubble growth above the PI film (Fig. 3a), whereas the die from the TO-247 package had some degradation in the silicon resistive layer with a dendrite-like pattern formation (Fig. 3b). After PI removal, the resistive layer was found to have eroded in the region of the bubbles, demonstrating that the failure presents similar characteristics (Fig. 3c). For both devices, the degradation is located between the last metal field plate and the EQR. This area is also characterized by the maximum electric field, as expected from TCAD simulations for this FLR termination.

These preliminary experiments confirm the capability of the HV-THB test to highlight failures in both MTP and TO-247 packages and the important role of humidity in the degradation mechanisms in the presence of high electric fields.

Journal of Vacuum Science Technology B

PLEASE CITE THIS ARTICLE AS DOI: 10.1116/1.5121880

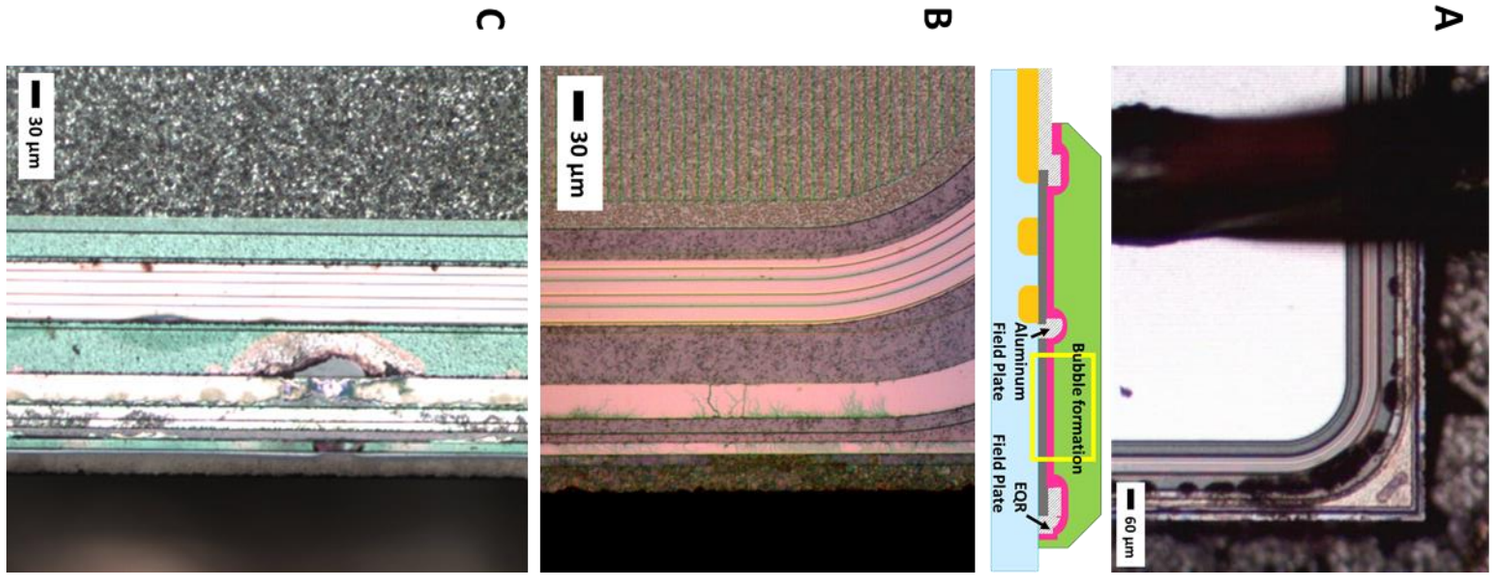

FIG. 3. (a) Optical microscope inspection (top view) of the device assembled in power module package after decapsulation, and termination scheme (cross-section) with localized bubble formation. Degradation occurs between the last metal field plate and the EQR field plate.

(b) Optical microscope inspection (top view) of a device assembled in TO-247 after gel removal. The silicon resistive layer presents a dendrite-pattern degradation between the last metal field plate and the EQR field plate.

(c) Optical microscope inspection (top view) of a failed device termination after PI removal. The resistive silicon is corroded between the last metal field plate and the EQR field plate.

III. RESULTS AND DISCUSSION

A. Preliminary experiment: polymer material passivation

In the failure analysis discussed in the previous section, the first sign of degradation was the presence of bubbles in the PI layer. This has led to different types of commercially available organic polymers being investigated as secondary passivation materials. Organic passivation refers to high-temperature thermosetting engineered polymers that have superior thermal stability (up to 450°C), excellent chemical and mechanical resistance, high adhesion to various materials, and excellent dielectric properties. The two families of commercially available polymers tested in this study are PBO and PI, which have low dielectric constants and high breakdown voltage capabilities.

From a materials point of view, PI has mechanical properties that guarantee high flexibility, high elongation before breaking, high tensile strength, and guaranteed thermal stability with a high T_g (glass transition). However, PI suffers from high moisture uptake (from 0.8–1.8% over 24 h at 23°C and 50% RH). Conversely, PBOs, are characterized by a smaller water uptake (0.5–0.7% over 24 h at 23°C and 50% RH) because of the absence of the carbonyl group, but in turn have less flexibility and lower resistance to stress with respect to PI.

The goal of the tests was to investigate new photosensitive (PS) PIs that can be easily integrated into photo-pattern processes and are more environment-, health-, and safety-friendly, with no normal methyl pyrrolidone solvent. This type of polymers contains catalysts, photo-initiators, and adhesion promoters that modify their composition. For this reason, proper solvent evaporation and complete imidization are key factors in enhancing their adhesion and chemical, mechanical, and T_g properties.[7] Thus, a setup that enables fine-tuning is fundamental.

As the degraded devices exhibit bubble formation in the PI layer, it is important to evaluate the adhesion and strength of this layer. Moreover, to exclude the influence of the deposition and enable process optimization, it is necessary to develop a set of rapid and efficient stress tests for such polymers that could be used in situ.

Therefore, the following empirical chemical stress tests were performed:

(i) Sulfuric stress test: 1-h immersion in concentrated sulfuric acid (H_2SO_4 96%) at 20ºC followed by visual evaluation.

(ii) Nitric stress test: 10-min immersion in concentrated nitric acid (HNO_3 65%) at 60ºC followed by visual evaluation.

The results (Fig. 4a) indicate that the PS PI displayed good resistance, with only small voids after the nitric acid test. The non-PS PI (Fig. 4b) also demonstrated excellent resistance, with only a light discoloration. PBO-based materials, however, showed more significant signs of degradation after both acid stress tests, evidencing lower chemical and mechanical resistance (Fig. 4c). Facets and cracks are clearly visible after the sulfuric acid test, while the film appears to have swelled and peeled off after the nitric acid stress test.

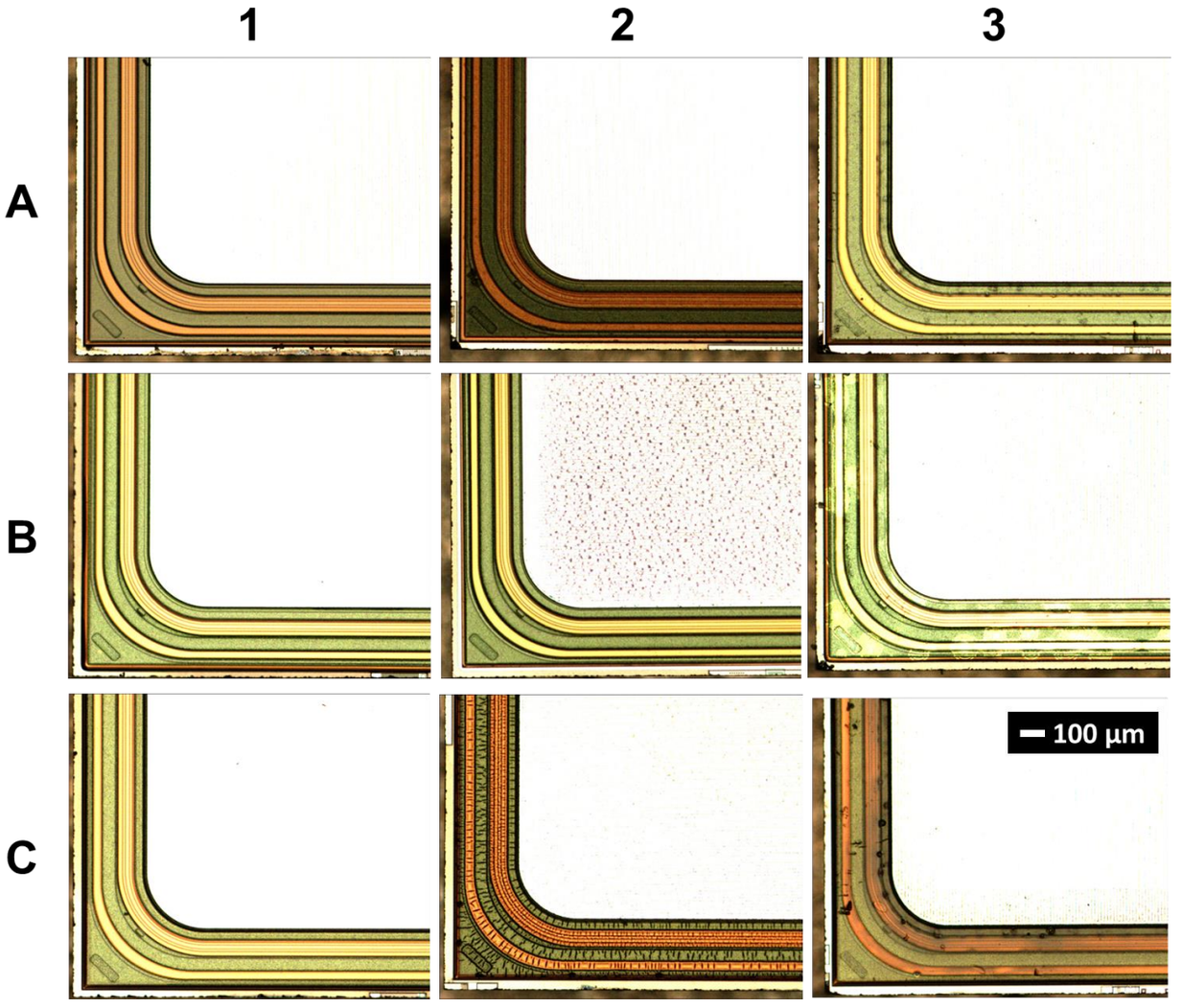

FIG. 4. Optical microscope inspection before and after sulfuric and nitric acid stress tests. Before stress tests: (1a) PS PI; (1b) non-PS PI; (1c) PS PBO. After sulfuric acid stress test: (2a) PS PI; (2b) non-PS PI; (2c) PS PBO. After nitric acid stress test: (3a) PS PI; (3b) non-PS PI; (3c) PS PBO.

After these chemical tests, three sets of 650 V power diodes were fabricated with the same primary passivation structure of silicon oxide, plus a resistive layer and one of three different polymers (non-PS PI, PS PI, and PS PBO), and assembled in a power module

package. To evaluate the polymer behavior, the three sets of samples were subjected to HV-THB test for 200 h with an applied voltage of 520 V, corresponding to 80% of the BV (Breakdown Voltage) device capability.

After silicone gel removal, optical microscope inspection, revealed polymer degradation with bubble formation in all three materials. An SEM image of an FIB cross-section, performed on a bubble in the failed termination area, highlights that the organic materials have not degraded, but have instead lifted, possibly a result of corrosion of the underlying layer of resistive silicon and of the aluminum field plate.[9] Indeed, the aluminum field plate appears swollen, with a change in conformity near the edge (Fig. 5).

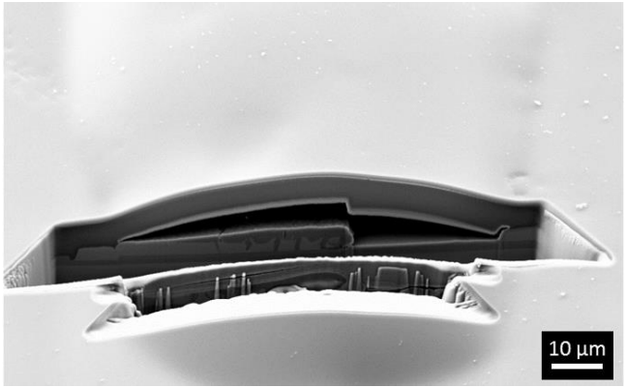

FIG. 5. SEM image of an FIB cut of a bubble in the failed termination area of the device. The PI has lifted and the aluminum has a modified appearance.

Moreover, from SEM imaging, the PI seems to maintain its adhesion with a very thin portion of the underlying film, but any deterioration in the latter could have induced a detachment, probably stimulated by the gas formation that caused the swelling.

B. Humidity adsorption: electrochemical phenomena

EDX analysis was performed to evaluate the change in composition along the aluminum field plate. Comparing data acquired from untouched aluminum portions and on degraded ones, it was possible to observe the appearance of different peaks. The presence of silicon can be explained by migration from the upper silicon resistive layer with the formation of aluminum silicide. Instead, the oxygen peak demonstrates the formation of aluminum oxide species.

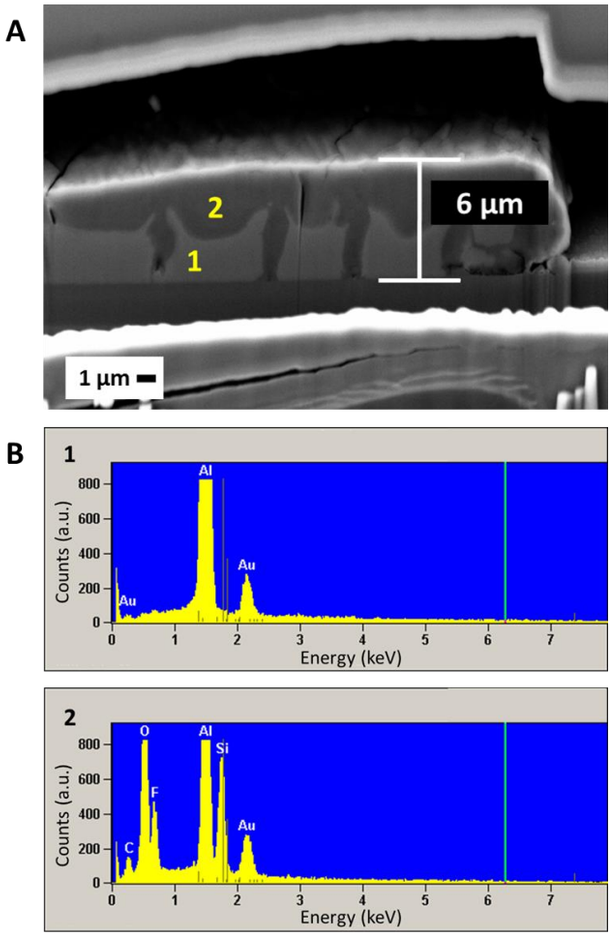

FIG. 6. (a) SEM image of an FIB cut across the aluminum field plate, for DUTs having P-doped oxide, after 200 h of testing. (b) EDX analysis on two different points of the aluminum field plate: 1) untouched portion 2) degraded portion. EDX spectra comparison reveals AlO_x and aluminum silicide formation (migration from resistive layer). Peaks of fluorine and carbon can be attributed to previous plasma etching (with SF_6) or cleaning (diluted HF) processes, and to the presence of organic materials such as PI.

These species derive from a combination of humidity penetration, electrochemical phenomena, and the high chemical reactivity of aluminum with water. More specifically, when water is adsorbed and an external bias is applied, a pH gradient forms due to the separation of H^+ and OH^- ions. In this environment, different types of reactions can occur. The general behavior for metal atoms in these conditions is as follows:

$$M \rightarrow M^{n+} + ne^- \text{ at the anode} \quad (1)$$

$$M^{n+} + ne^- \rightarrow M \text{ at the cathode} \quad (2)$$

Reaction (2) is usually accompanied by dendrite formation along the surface of the material involved in the metal transportation[4] (see Fig. 3b for an example of dendrite formation).

Aluminum, which is typically used as a contact metal in this type of device, is known to be particularly reactive in the conditions previously explained. In fact, aluminum easily forms hydroxides when in contact with water. These compounds are

quite stable in neutral solutions, but in the presence of acids or bases, they dissolve rapidly, resulting in layer corrosion.

The proposed reactions that are occurring are as follows:

$$Al + 3H_2O \rightarrow Al(OH)_3 + 3/2H_2 \quad (3)$$

(overall reaction of aluminum with water)

In neutral environments, $Al(OH)_{3(amorphous)}$ is transformed to the stable hydrated oxide:

$$Al(OH)_3 \rightarrow Al_2O_3 \cdot H_2O$$

which has a free energy of formation of -436.3 kcal, and acts as a passivated barrier.

Alkaline solutions are able to destabilize this protective oxide that forms AlO_2^-,[10] and can therefore cause rapid dissolution of aluminum at room temperature, which continues to react and consume water following Eq. (3). In high-humidity conditions, this equilibrium is completely right-shifted, causing H_2 formation, which could explain the spongy appearance of the aluminum layer and polyimide bubble formation.

C. Humidity absorption: the influence of inner layers

All power diodes manufactured with organic polymer (PI) passivation in direct contact with the resistive silicon layer exhibit degradation after HV-THB tests. As humidity penetration is one of the most influential factors in semiconductor device degradation,[8] experimental tests were conducted to study the moisture absorption of the silicon resistive layer when deposited on different (doped or non-doped) oxide layers.

The presence of elements such as boron and phosphorous in borophosphosilicate glass and phosphosilicate glass increases the hygroscopicity of the silicon resistive film that is deposited on top. Contact angle measurements performed on the resistive layer deposited on P-doped low thermal oxide confirm the high surface wettability and sharp angle drop shape. The same measurements performed on the silicon resistive layer deposited on undoped materials instead show a more hydrophobic behavior (see Table I).

TABLE I. Contact angle measurements on resistive silicon deposited on doped and undoped oxide.

Calculated angles for water drop on Si resistive layer over:	
A) Doped oxide	32.6°
B) Undoped oxide	46.4°

D. Complete passivation evaluation: SiO_2–Si_3N_4 capping layer

To complete a systematic study, a final test was performed by adding two reinforcing capping layers of PECVD (Plasma-Enhanced Chemical Vapor Deposition) silicon nitride and PECVD silicon dioxide to complete the passivation structure.

For this purpose, two sets of 650 V power diodes, having the same primary passivation structure of silicon oxide plus resistive layer, were produced by adding either a silicon dioxide (sample A) or a silicon nitride (sample B) interlayer with the same thickness. The diodes were completed with PS PI (Fig. 7).

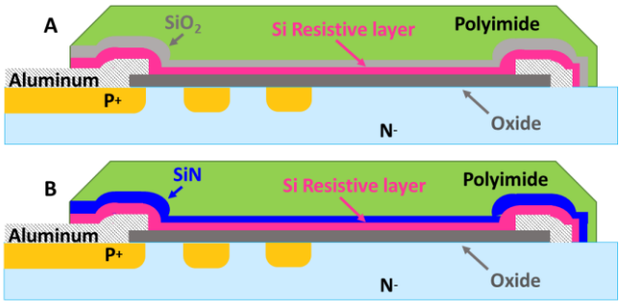

FIG. 7. Passivation details: SiO_2 capping layer (sample A) and Si_3N_4 capping layer (sample B) applied to a typical planar HV termination.

After fabrication and assembly in MTP power modules, the devices were stressed by performing HV-THB tests at 85°C, 85% RH, with 520 V applied bias (V_r at 80% of rated voltage capability). These tests focused on evaluating two different complete passivation structures, in which the samples had the same first level passivation, but different secondary passivation.

Before and after each step of the HV-THB tests, the DUTs were subjected to I-V analysis of the diode reverse characteristics. In particular, the devices with a silicon nitride capping layer did not exhibit any shift or significant electrical characteristic variation, presenting a stable leakage current level up to 1500 h. In contrast, the devices with a SiO_2 capping layer displayed a leakage shift above the imposed threshold after 750 h, and so the test was stopped before further deterioration.

After device decapsulation, failure analysis proceeded with an optical inspection of the selected DUTs. Optical microscope evaluation of the SiO_2 samples, which failed

after 750 h, seemed to evidence no physical change in the device structure. As expected, the same result was obtained for the silicon nitride samples, which were still presenting good electrical characteristics after 1500 h. However, an in-depth observation performed with SEM on an FIB cut of the DUTs that failed after 750 h highlighted small voids in the Si resistive layer and on the capping oxide (Fig. 8a). After further inspections, we can link the leakage degradation to the morphological variation of the interface between the oxide capping layer and the silicon resistive layer.

Figure 8b shows the SEM image of an FIB cut of a silicon nitride sample that still showed good electrical characteristics after 1500 h of the HV-THB test. There is no sign of any physical degradation.

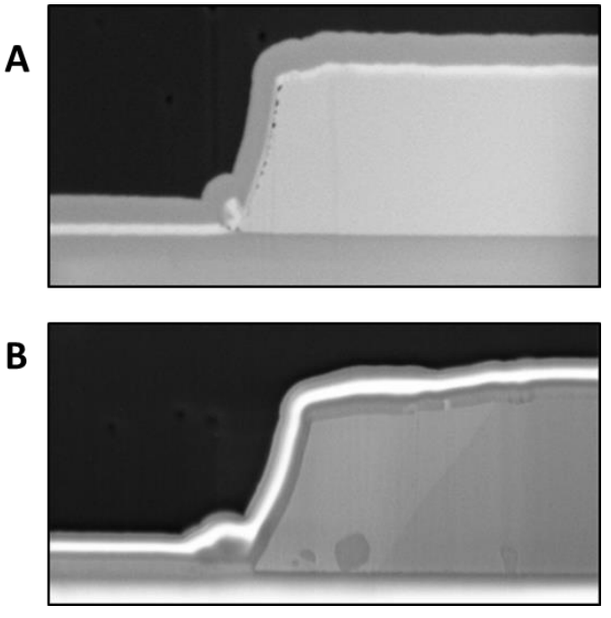

FIG. 8. (a) SEM image of an FIB cut of SiO_2 DUT that failed after 750 h. Small voids on the Si resistive layer and on the oxide capping interface are evident.

(b) SEM image of an FIB cut of silicon nitride DUT that showed good electrical characteristics after 1500 h of HV-THB testing. No signs of variation are present between the passivation layers.

IV. CONCLUSIONS

A systematic approach has been used to study and validate the complex termination–passivation plurality using a new HV-THB stress test. The capability of this new HV-THB test to stress devices and highlight specific failure modes has been proved.

The interaction between high voltage and humidity at high temperature has been found to be the most stressful factor for passivation materials. This is particularly evident in specific termination areas subjected to high electric fields, which clearly exhibit deterioration after testing. For these reasons, it is important to enhance the reliability and robustness of power devices, especially those operating under high stress and in harsh working conditions, such as in power module applications.

This study, combined with TCAD design optimization, has helped to validate the design of certain devices, leading to optimized passivation structures for these purposes.

ACKNOWLEDGMENTS

The authors are grateful to the Department of Applied Science and Technology at the Polytechnic University of Turin for their support in SEM/FIB analysis, and to Vishay Semiconductors Italiana S.P.A. Reliability Laboratory, Failure Analysis Laboratory, and Manufacturing and Assembly Departments for their efforts and resources invested in this work. Furthermore, the authors would like to thank all colleagues from Vishay Semiconductors Italiana S.P.A. and the Polytechnic University of Turin.

REFERENCES

[1]S. Kremp and O. Schilling, Microelectron. Reliab. **89-90**, 447 (2018).

[2]J. Jormanainen, E. Mengotti, T. B. Soeiro, E. Bianda, D. Baumann, T. Friedli, A. Heinemann, A. Vulli, and J. Ingman, "High Humidity, High Temperature and High Voltage Reverse Bias - A Relevant Test for Industrial Application," PCIM, Nuremberg, Germany (2018).

[3] U. Grossner, A. Mihaila, and U. Vemulapati, ECS Trans. **50**, 267 (2013).

[4] C. Zorn and N. Kaminski, "Temperature Humidity Bias (THB) Testing on IGBT Modules at High Bias Levels," CIPS, Nuremberg, Germany (2014).

[5] C. Zorn and N. Kaminski, "Acceleration of Temperature Humidity Bias (THB) Testing on IGBT Modules by High Bias Levels," ISPSD, Hong Kong (2015).

[6] D. Cimmino, R. Busca, S. Ferrero, F. Pirri, G. Richieri, and R. Carta, Microelectron. Reliab. **100-101**, 113319 (2019).

[7] Automotive Electronics Council, Stress Test Qualification for Automotive Grade Discrete Semiconductors, AEC-Q101-Rev-D1 (2013).

[8] W. Chen, W. Chen, B. Zhang, S. Yang, and C. Y. Liu, Polym. **109**, 205 (2017).

[9] C. Papadopoulos, C. Corvasce, A. Kopta, D. Schneider, G. Pâques, and M. Rahimo, Microelectron. Reliab. **88-90**, 470 (2018).

[10] H. Z. Wang, D. Y. C. Leung, M. K. H. Leung, and M. Ni, Renew. Sust. Energ. Rev. **13**, 845 (2009).

Journal of Vacuum Science Technology B

PLEASE CITE THIS ARTICLE AS DOI: 10.1116/1.5121880

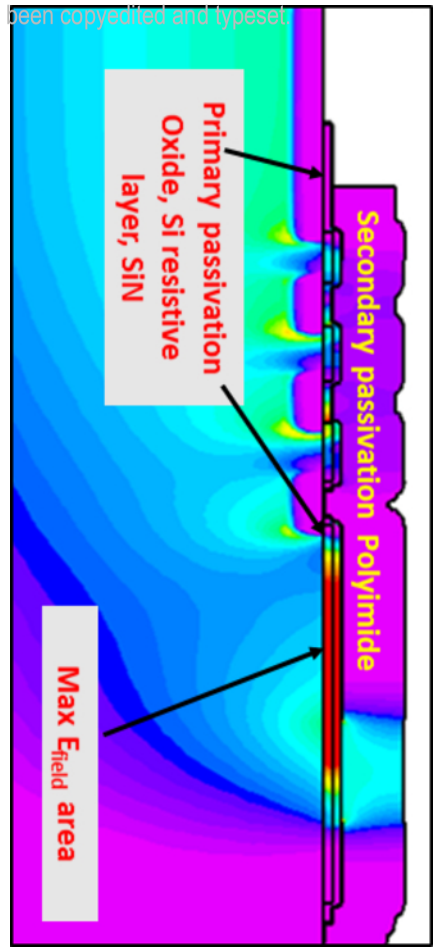

Journal of Vacuum Science Technology B

PLEASE CITE THIS ARTICLE AS DOI: 10.1116/1.5121880

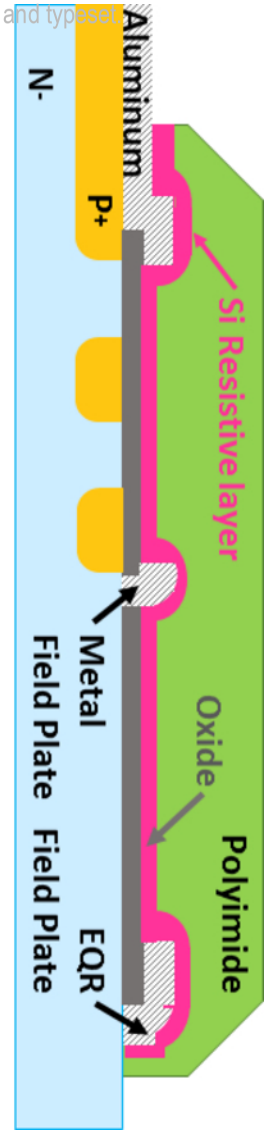

Journal of Vacuum Science Technology B

Journal of Vacuum Science Technology B

PLEASE CITE THIS ARTICLE AS DOI: 10.1116/1.5121880

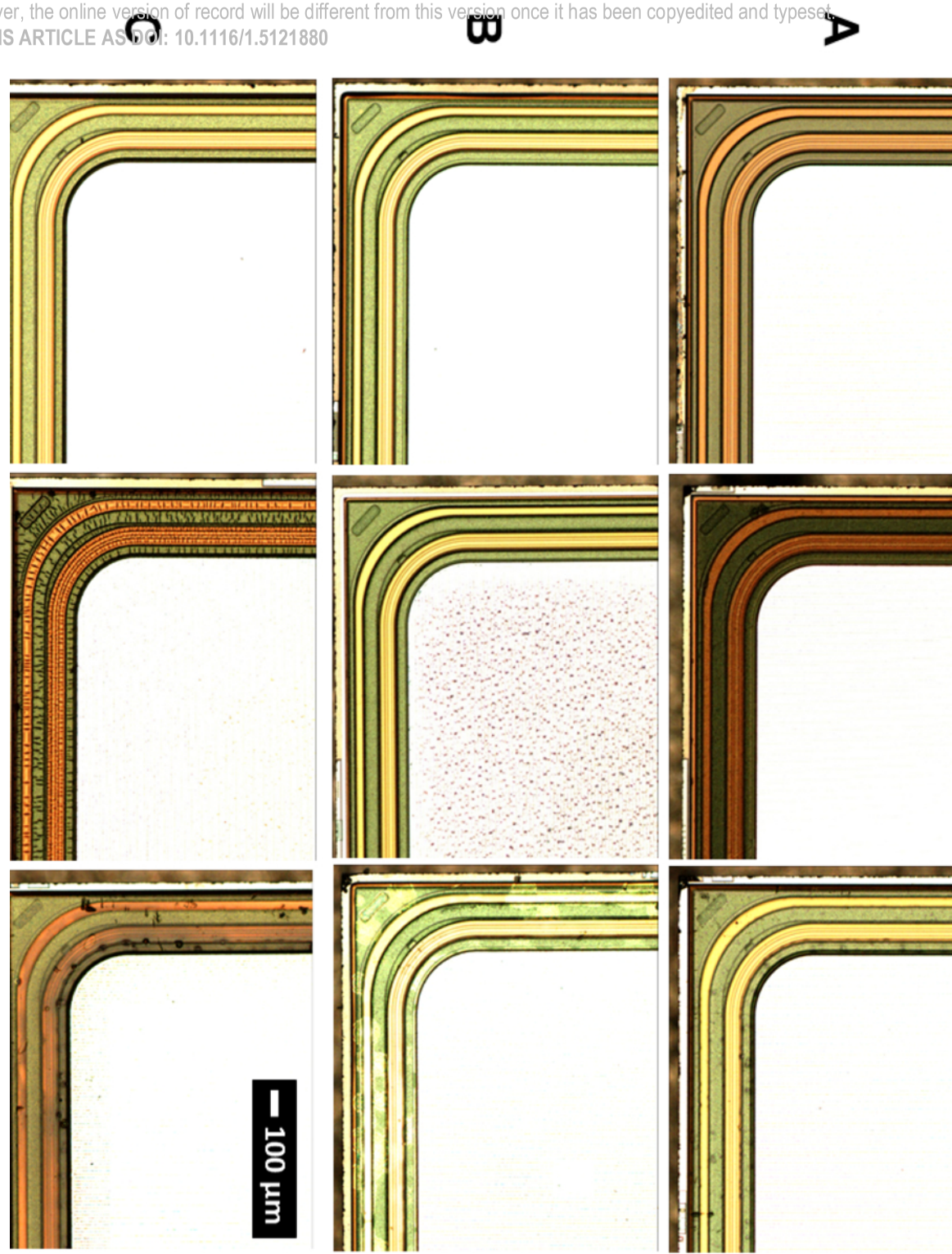

Journal of Vacuum Science Technology B

PLEASE CITE THIS ARTICLE AS DOI: 10.1116/1.5121880

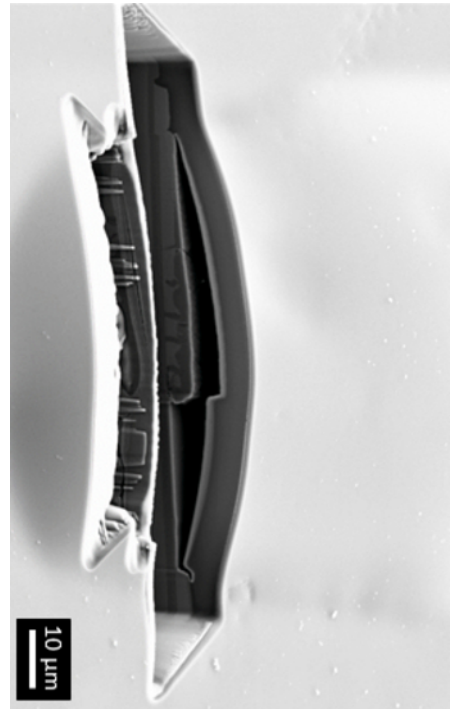

Journal of Vacuum Science Technology B

Journal of Vacuum Science Technology B

PLEASE CITE THIS ARTICLE AS DOI: 10.1116/1.5121880

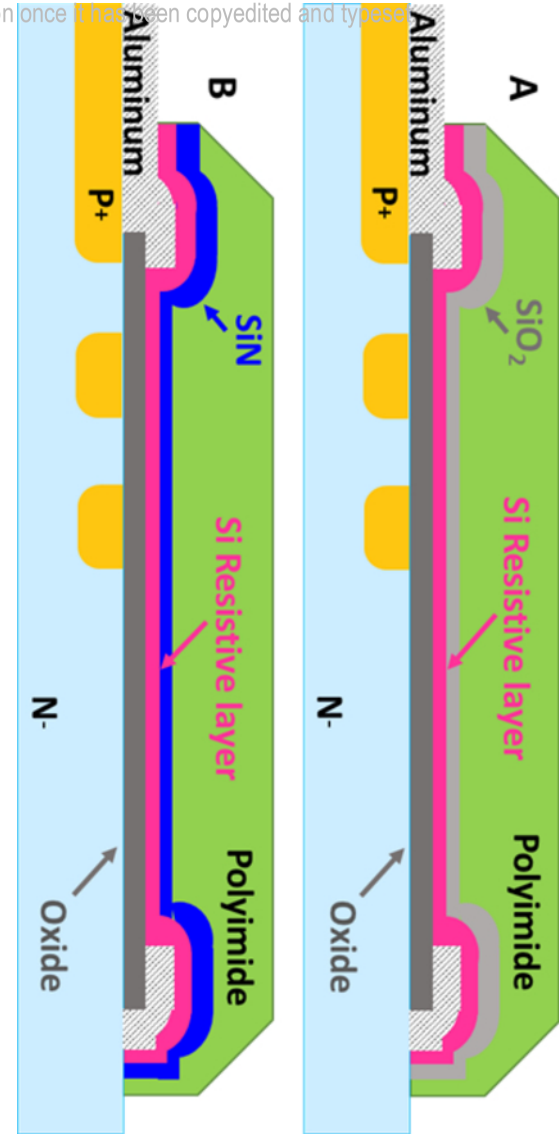

Journal of Vacuum Science Technology B

PLEASE CITE THIS ARTICLE AS DOI: 10.1116/1.5121880